

QUANTUM PHASE TRANSITION FROM A STRANGE METAL TO A FERMI LIQUID IN THE NORMAL STATE OF CUPRATE SUPERCONDUCTORS

ANDREW DAS ARULSAMY

ABSTRACT. The normal state metallic behavior above the superconducting transition temperature (T_{sc}) remains one of the least understood properties since its discovery in cuprates by Bednorz and Müller [1]. Apart from the pseudogap (T^*) phenomenon above T_{sc} , there is this T -linear resistivity that was first recognized by Anderson [2] as strange simply because it does not obey the low-temperature T^2 electron-electron scattering rate predicted from the Fermi liquid theory. Here, we prove that the finite temperature continuous quantum phase transition (C_T QPT) is responsible for the transition from a strange metal to a Fermi liquid for a given chemical composition. Our proof follows the Green function formalism and the energy-level spacing renormalization group method. Interestingly, the C_T QPT stated above can be related to the proof derived by Parameswaran, Shankar and Sondhi [3], in which, the one-to-one correspondence between the Fermi gas and Fermi liquid is indeed a special case. The theory is further exploited to give unambiguous explanations as to why and how doping gives rise to spectral weight transfer observed in the soft X-ray absorption spectroscopic measurements for the La-Sr-Cu-O system.

PACS: 74.72.-h, 71.10.Hf, 74.25.F-, 74.25.Jb

1. INTRODUCTION

Landau's Fermi liquid theory (FLT) was originally developed to explain the liquid state of Helium-3. Later, it was applied to explain the free-electron metals (with one-to-one correspondence between FLT and free-electrons), where it has fulfilled its purpose with unprecedented accuracies such that its predictions are qualitatively comparable with experiments [4, 5, 6, 7, 8]. However, the knowledge derived from FLT is found to be inadequate (not inaccurate) to explain certain metals with strongly interacting electrons. For example, the metallic property of heavy fermions and high temperature superconductors above the critical transition temperature do not obey FLT [9, 10]. When one comes to think of it, this is not surprising at all because the metallic behavior of strongly-interacting electrons, physically should not obey the non-interacting fermions (or Fermi gas). On the other hand, any new theory put forward to explain the metallic property in the presence of strong interaction(s) will have to be inadequate to explain the free-electron metals, which is a necessary condition. This condition is necessary because removing or adding this interaction Hamiltonian ($H_{int}(x)$) is always *by hand*, even if it is done with appropriate limits ($H_{int}(x) \rightarrow 0$ or $x \rightarrow \infty$), where x is some parameter inversely proportional to the interaction strength. Such theoretical inadequacies (between FLT and the prospective theory) imply the existence of a quantum phase transition

Date: September 29, 2011.

due to changing chemical composition via doping (above and/or below a certain critical temperature). Details on the zero temperature quantum phase transition ($0K$ QPT) due to changing pressure, doping and magnetic fields, and Mott-Hubbard transition are given in Refs. [11, 12, 13, 14, 15, 16, 17].

There are other types of critical temperatures such as the superconducting (and the pseudogap) transition temperatures (T_{sc} and T^*) for cuprates, the Curie temperature (T_C) for ferromagnets, the Neel temperature (T_N) for antiferromagnets, or the ferroelectric transition temperature (T_{fc}) for ferroelectrics, in addition to the metal-to-insulator transition temperature. Here, a new critical phenomenon is proven to exist, which can be associated to the continuous finite temperature quantum phase transition (T QPT). For example, from a strongly interacting metal (a strange metal) to a Fermi metal. However, there is an important exception, in which, the T QPT developed and proven in this work does not include the superconductor transition temperature and the pseudogap phase in any way. As such, the T QPT must be above (not below) the T^* if $T_{sc} < T^*$. The term “non-metals” means semiconductors or insulators such that the electrons in the conduction or overlapped band cannot be treated as free-electrons. The superconducting phase and the regime in its vicinity above T_{sc} has been deliberately excluded because we are not sure (beyond any doubt) how the energy level spacing of a given compound evolve with chemical doping to give rise to superconductivity (this work is in progress).

In the early days of the ionization energy theory (IET), it is true that we have developed resistivity models for cuprates for all temperatures between T_{sc} (including T^*) and room temperature using exotic particles (due to charge-spin separation [2, 18, 19, 20]), namely, spinons (uncharged electrons) and holons (spinless charged bosons) [21, 22]. A proof is also developed (using the Ioffe-Larkin conductivity rule [23]) to justify the above models by invoking the co-existence of electrons, spinons and holons [24]. However, the theory developed and proven here is entirely based on the strongly correlated electrons within IET and the Green function formalism, without requiring such exotic particles. For the records, IET is not a non-Fermi liquid theory. In particular, these strongly correlated electrons require certain additional conditions compared to the well-known Fermi liquid theory and the Fermi gas concept. In view of this, indeed, we have been unfaithful and have switched side (back to electrons) after the discovery of (i) the pseudogap-like features in manganites [25] and (ii) the existence of $\xi \neq 0$ even in the presence of crossed energy levels [26]. To make sure the readers and I are in resonance, a new Section (Further analysis) is added toward the end, to iron out any unclear issue that may have left unexplained.

Our main conclusions are as follows; (a) the phase transition from a strange metal to the Fermi liquid is due to the finite-temperature continuous quantum phase transition (QPT) as a result of the insignificant effect from the energy-level spacing, (b) Fermi gas is a special case having a one-to-one correspondence with the Fermi-liquid if the energy-level spacing is zero, (c) the spectral weight transfer due to doping in cuprates observed in the soft X-ray absorption spectroscopic measurements can be unequivocally captured with the Green function developed within IET, and (d) the emergent phenomenon put forth by Anderson [27] can be related to quantum phase transitions.

2. RENORMALIZED GREEN FUNCTION

Before we explore the electronic phase transitions in superconducting cuprates above T_{sc} , we first need to renormalize the relevant interaction term in the Hubbard Hamiltonian via the energy-level spacing renormalization technique within the Green function formalism. The reason for doing this is to expose any interesting electronic phase transition due to crossed energy-levels, giving rise to overlapped bands such that $\xi \neq 0$. However, the free-electron metallic phase is well-known to exist in the overlapped region, which satisfies the weakly-interacting Fermi liquid that has a one-to-one correspondence with the Fermi gas when the Mott-Hubbard gap (U_H) closes and $\xi = 0$. The conditions $U_H = 0$ and $\xi \neq 0$ can be understood by noticing that the energy-level crossings at a certain \mathbf{k} -point, say at \mathbf{k}_1 may imply $E_a(\mathbf{k}_1) = E_b(\mathbf{k}_1)$ but $\xi \neq 0$ due to interactions where E_a and E_b are the eigenvalues for the solved two-level Hamiltonian

$$\begin{aligned} H(\mathbf{k})\varphi_a(\mathbf{k}) &= [H_0(\mathbf{k}) + \mathcal{V}(\mathbf{k})]\varphi_a(\mathbf{k}) = [h_a(\mathbf{k}) + v_a(\mathbf{k})]\varphi_a(\mathbf{k}) = E_a(\mathbf{k})\varphi_a(\mathbf{k}), \\ (2.1) \quad H(\mathbf{k})\varphi_b(\mathbf{k}) &= [H_0(\mathbf{k}) + \mathcal{V}(\mathbf{k})]\varphi_b(\mathbf{k}) = [h_b(\mathbf{k}) + v_b(\mathbf{k})]\varphi_b(\mathbf{k}) = E_b(\mathbf{k})\varphi_b(\mathbf{k}). \end{aligned}$$

Here, $H_0(\mathbf{k})$ is the basic Hamiltonian excluding all interactions, whereas $\mathcal{V}(\mathbf{k})$ contains all the interaction terms, and we do not impose any condition like $\langle \varphi_a(\mathbf{k}) | \varphi_b(\mathbf{k}) \rangle = 0$ or 1. Obviously we have $E_a(\mathbf{k})$, $h_a(\mathbf{k})$, $v_a(\mathbf{k})$, $h_b(\mathbf{k})$, $v_b(\mathbf{k})$ and $E_b(\mathbf{k})$ as eigenvalues. Degeneracy due to energy level crossing in \mathbf{k} -space implies $E_a(\mathbf{k}_1) = E_b(\mathbf{k}_1)$ at a certain \mathbf{k} point (\mathbf{k}_1), and at other \mathbf{k} points, they are not degenerate. If they are always degenerate, then $h_a(\mathbf{k}) = h_b(\mathbf{k})$, $v_a(\mathbf{k}) = v_b(\mathbf{k})$ and $E_a(\mathbf{k}) = E_b(\mathbf{k})$, which physically mean $\varphi_a(\mathbf{k}) = \varphi_b(\mathbf{k})$: this strictly implies that there are two electrons occupying the degenerate energy level throughout the \mathbf{k} -space ($U_H = 0$ and $\xi = 0$). As a consequence, degeneracy due to energy level crossing requires $h_a(\mathbf{k}_1) \neq h_b(\mathbf{k}_1)$, $v_a(\mathbf{k}_1) \neq v_b(\mathbf{k}_1)$ and $E_a(\mathbf{k}_1) = E_b(\mathbf{k}_1)$, i.e., $U_H = 0$ and $\xi \neq 0$. The above logical exposition originates from Ref. [26].

2.1. Green function formalism. The main feature of the Green function formalism is due to its suitability to describe electronic properties of the interacting electrons [28, 29, 30]. The Green function,

$$(2.2) \quad \mathcal{G}(t - t') = -\frac{i}{\hbar} \theta(t - t') \langle \{c_\alpha(t), c_\alpha^\dagger(t')\} \rangle,$$

defines the probability amplitude of finding a particle at a later time, t in the state, $\alpha = \mathbf{n}\mathbf{k}\sigma$, in which the particle was actually created at an initial time, t' where $t > t'$, \mathbf{n} is the principal quantum number and σ denotes spin-up ($\sigma, \sigma', \uparrow, +\frac{1}{2}$) or down ($-\sigma, -\sigma', \downarrow, -\frac{1}{2}$). Here, $c_\alpha(t)$ and $c_\alpha^\dagger(t)$ denote the usual annihilation and creation operators for fermions, while the curly bracket denotes anti-commutator. Moreover,

$$(2.3) \quad \theta(t - t') = \int \delta(t - t') dt.$$

Hence, the Green function given in Eq. (2.2) captures the propagation of an electron during the time interval from t' to t [28]. By taking the time derivative of Eq. (2.2), one can show that [28]

$$(2.4) \quad i\hbar \frac{\partial \mathcal{G}(t - t')}{\partial t} = \delta(t - t') - \frac{i}{\hbar} \theta(t - t') \langle \{[c_\alpha(t), H], c_\alpha^\dagger(t')\} \rangle,$$

where H is the many-body Hamiltonian. If H is the free-electron (non-interacting) Hamiltonian, then the Fourier transformed Green function [also known as the free propagator with superscript (0)] is given by [28, 29]

$$(2.5) \quad \mathcal{G}^{(0)}(E) = \frac{1}{E - E_\alpha + i\delta},$$

where, δ is a convergence parameter. Equation (2.5) has a pole when $E - E_\alpha + i\delta = 0$ and the density of states is $\sum_\alpha \delta(E - E_\alpha)$, where $\delta(E - E_\alpha)$ is a delta function. If the interaction is included, say, the e - e interaction, then Eq. (2.5) can be written as [28, 29]

$$(2.6) \quad \mathcal{G}(E, \Sigma) = \frac{1}{E - [E_\alpha + \Sigma(\alpha, E)] + i\delta}.$$

Therefore, there is an additional energy term in the presence of e - e interaction that changes the pole structure (spectra), which is known as the self-energy correction $[\Sigma(\alpha, E)]$. In principle, Eq. (2.6) captures the overall structure of the solution with many-body interaction [28, 29]. Importantly, Eq. (2.5) (without interaction) and Eq. (2.6) are identical mathematically with $E_\alpha + \Sigma(\alpha, E)$ as the effective many-body electronic energy.

2.2. Hubbard model. The Hubbard model [16, 17] is unique in a sense that it was the first model used to interpret the insulating property in transition metal oxides. The Hubbard model Hamiltonian [28]

$$(2.7) \quad H^H = E^{(0)} \sum_{\mathbf{R}, \sigma} c_{\mathbf{R}\sigma}^\dagger c_{\mathbf{R}\sigma} + \mathfrak{t} \sum_{\mathbf{R}+\mathbf{d}, \sigma} c_{\mathbf{R}+\mathbf{d}\sigma}^\dagger c_{\mathbf{R}\sigma} + U_H \sum_{\mathbf{R}} n_{\mathbf{R}\uparrow} n_{\mathbf{R}\downarrow}.$$

Here, $n_{\mathbf{R}\uparrow}$ and $n_{\mathbf{R}\downarrow}$ are the number operators with spin-up and spin-down, respectively, $E^{(0)}$ is the non-interacting atomic energy level, \mathbf{R} is the lattice-point coordinate, and \mathbf{d} is the distance between two nearest ions with certain spin configuration. The hopping or transfer matrix elements between the two nearest neighboring sites $(\mathbf{R}, \mathbf{R} + \mathbf{d})$ is [28]

$$(2.8) \quad \mathfrak{t} = \int d^3\mathbf{r} \phi^*(\mathbf{r}) \mathbf{v}(\mathbf{r}) \phi(\mathbf{r} - \mathbf{d}),$$

where $\phi(\mathbf{r})$ and $\phi(\mathbf{r} - \mathbf{d})$ denote the spin-independent (neglected spin-orbit coupling) atomic-like orbitals at sites \mathbf{R} and $\mathbf{R} + \mathbf{d}$, respectively, which are distorted in the crystalline environment, and $\mathbf{v}(\mathbf{r}) = (e^2/4\pi\epsilon_0)(1/|\mathbf{r}| + 1/|\mathbf{r} - \mathbf{d}|)$ is the Coulomb potential due to those two lattice sites (See Fig. 1(A)).

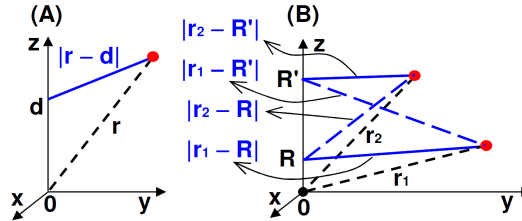


FIGURE 1. (A) and (B) depict the coordinates used to write Eqs. (2.8) and (2.9), respectively.

The interaction matrix elements [28]

$$(2.9) \quad \mathcal{V}_{\mathbf{R}\mathbf{R}'} = \frac{1}{2} \int \phi^*(\mathbf{r}_1 - \mathbf{R}) \phi^*(\mathbf{r}_2 - \mathbf{R}) \frac{e^2 d^3 \mathbf{r}_1 d^3 \mathbf{r}_2}{4\pi\epsilon_0 |\mathbf{r}_1 - \mathbf{r}_2|} \phi(\mathbf{r}_2 - \mathbf{R}') \phi(\mathbf{r}_1 - \mathbf{R}'),$$

gives the Mott-Hubbard gap, U_H , and the coordinates are shown in Fig. 1(B). In writing Eq. (2.9), we considered the Hamiltonian that describes the two static ions and the two-electron interaction, which is a reasonable approximation when one only considers the nearest neighbors [28]. In this case, the interaction Hamiltonian [28] (from Eqs. (2.7) and (2.9))

$$(2.10) \quad H_{\text{int}}^H \approx \sum_{\mathbf{R}, \sigma, \mathbf{R}', \sigma'} \mathcal{V}_{\mathbf{R}\mathbf{R}'} c_{\mathbf{R}\sigma}^\dagger c_{\mathbf{R}'\sigma'}^\dagger c_{\mathbf{R}'\sigma'} c_{\mathbf{R}\sigma} = \sum_{\mathbf{R}, \sigma, \mathbf{R}', \sigma'} \mathcal{V}_{\mathbf{R}\mathbf{R}'} n_{\mathbf{R}\sigma} n_{\mathbf{R}'\sigma'}.$$

We have used $n_{\mathbf{R}\sigma} = c_{\mathbf{R}\sigma}^\dagger c_{\mathbf{R}\sigma}$, where $\mathbf{R}\sigma \neq \mathbf{R}'\sigma'$, which means $c_{\mathbf{R}\sigma}^\dagger c_{\mathbf{R}'\sigma'} = 0$. If $\sigma = \uparrow, \sigma' \rightarrow -\sigma' = \downarrow$ and $\mathbf{R} = \mathbf{R}'$, then electron \mathbf{r}_1^\downarrow (electron at \mathbf{r}_1 with spin down) and \mathbf{r}_2^\uparrow can occupy the same site \mathbf{R} , which then leads Eq. (2.9) to be written as

$$(2.11) \quad \sum_{\mathbf{R}, \mathbf{R}'} \mathcal{V}_{\mathbf{R}\mathbf{R}'} = \sum_{\mathbf{R}} \mathcal{V}_{\mathbf{R}\mathbf{R}} = U_H.$$

The Green function based on the Hamiltonian given in Eq. (2.9), *in the atomic limit* is [28]

$$(2.12) \quad \mathcal{G}(E, U_H) = \frac{1 - \langle n_{-\sigma} \rangle}{E - E^{(0)} + i\delta} + \frac{\langle n_{-\sigma} \rangle}{E - [E^{(0)} + U_H] + i\delta}.$$

Equation (2.12) gives two poles where the first pole at $E^{(0)}$ is due to $E - E^{(0)} + i\delta = 0$ and the second pole at $E^{(0)} + U_H$ is from $E - [E^{(0)} + U_H] + i\delta = 0$.

2.3. IET and the Mott-Hubbard metal-insulator transition. The advantages of invoking the Hubbard model within the ionization energy theory are four-fold, namely,

(i) We will understand that the screened Coulomb potential for a two-electron system, \hat{V}_{sc} (Eq. (19) of Ref. [31]) captures the same effect as the Mott-Hubbard gap, U_H , and it is in the form of Shankar-type screened Coulomb potential [32], which is

$$(2.13) \quad \hat{V}_{\text{sc}} = \frac{e^2}{4\pi\epsilon_0 |\mathbf{r}_1 - \mathbf{r}_2|} e^{-\mu(r_1 + r_2) e^{\frac{1}{2}\lambda(-\xi)}},$$

where $\mu e^{\frac{1}{2}\lambda(-\xi)}$ denotes the screening parameter, μ is the constant of proportionality and $|\mathbf{r}_1 - \mathbf{r}_2| = \sqrt{r_1^2 + r_2^2 - 2r_1 r_2 \cos(\theta_2)}$. Here, $\lambda = 12a_B \pi \epsilon_0 / e^2$, a_B is the Bohr radius of atomic hydrogen, e and ϵ_0 denote the electron charge and the permittivity of free space, respectively.

(ii) Since the $\langle \hat{V}_{\text{sc}} \rangle$ is also a function of the ionization energy (ξ), one has the advantage of studying the evolution of $\langle \hat{V}_{\text{sc}} \rangle$ with respect to doping: strength of the metal-insulator transition due to doping or changing interaction strength, which is not straightforward with U_H .

(iii) To obtain the Green function as a function of the ionization energy, and

(iv) New conditions can be invoked such that $U_H = 0$ and $\xi \neq 0$ that do not satisfy the free-electron metals.

For an apparent reason, we have identified ξ interchangeably with the ionization energy and the energy-level spacing. The reason is that the existence of this energy-level spacing originated from the screening of the valence electron due to

some Coulomb repulsion from an inner electron, which can be observed in any two-electron atom or ions, namely, in He, Li^+ , Be^{2+} , and so on. For example, the Coulomb attraction between a valence electron and its nucleus will increase systematically from He to Li^+ and to Be^{2+} , which is why we need larger ionization energies (due to increasing Z) to remove them. At the same time, we also have a stronger Coulomb repulsion between those two electrons as a result of increasing Z , which have given rise to a larger energy-level spacing. Increasing Z means increasing Coulomb attraction between an electron and its nucleus. If $U_H = 0$ and $\xi = 0$, then the system is in a free-electron metallic phase. The new condition, $U_H = 0$ and $\xi \neq 0$ gives rise to the strange metallic phase in the normal state of cuprates. To see the similarity between U_H and ξ clearly, let us recall the interaction part of the Hubbard Hamiltonian [Eqs. (2.9) and (2.10)] here, in which, we can rewrite Eq. (2.9) using Eq. (2.13) to obtain

$$(2.14) \quad \langle \hat{V}_{\mathbf{R}\mathbf{R}'}^{\text{sc}} \rangle = \frac{1}{2} \int d^3\mathbf{r}_1 d^3\mathbf{r}_2 \phi^*(\mathbf{r}_1 - \mathbf{R}) \phi^*(\mathbf{r}_2 - \mathbf{R}) [\hat{V}_{\text{sc}}] \phi(\mathbf{r}_2 - \mathbf{R}') \phi(\mathbf{r}_1 - \mathbf{R}'),$$

where the atomic orbitals (ϕ) are exactly the same for both $\mathcal{V}_{\mathbf{R}\mathbf{R}'}$ in Eq. (2.9) (undoped) and $\hat{V}_{\mathbf{R}\mathbf{R}'}^{\text{sc}}$ in Eq. (2.14) (doped). Using Eq. (2.14), the renormalized Green function within IET is

$$(2.15) \quad \mathcal{G}(E, \langle V^{\text{sc}} \rangle) = \frac{1 - \langle n_{-\sigma} \rangle}{E - E^{(0)} + i\delta} + \frac{\langle n_{-\sigma} \rangle}{E - [E^{(0)} + \langle V_{\mathbf{R}\mathbf{R}}^{\text{sc}} \rangle] + i\delta}.$$

Therefore, we can now study the evolution of the Mott-Hubbard gap (the shifting of the poles) for various doping elements because $\langle V_{\mathbf{R}\mathbf{R}}^{\text{sc}} \rangle$ is a function of ξ , which in turn uniquely related to the type of elements in a given solid (non-free-electrons). In summary, the Hubbard model that gives rise to U_H as a result of e - e Coulomb repulsion has been recaptured within the IET by identifying that U_H is equivalent to $\langle V_{\text{sc}} \rangle$ in the atomic limit.

Figure 2 schematically captures the similarity between the Hubbard model and the IET. For example, for two-ion (A and B) and two valence electron system, the Hubbard model needs the accurate atomic orbitals for each electron to determine U_H . On the other hand, the IET captures the same scenario via $\langle V_{\mathbf{R}\mathbf{R}}^{\text{sc}} \rangle$, and on top of that, the evolution of $\langle V_{\mathbf{R}\mathbf{R}}^{\text{sc}} \rangle$ is also predictable for different ions substituting A and/or B. In other words, if we have a system, $\text{AB}_{1-x}\text{C}_x$, then one takes the average of ξ as follows; $\xi_{\mathbf{r}_2} = (1-x)\xi_B + (x)\xi_C$, which will evolve with the content of ion C that systematically substitutes B. As for the transfer matrix elements, \mathbf{t} [see Eq. (2.8)], one does not need to evaluate this parameter since it is straightforward to notice the relation, $\mathbf{t} \propto 1/U_H \propto 1/\langle V_{\mathbf{R}\mathbf{R}}^{\text{sc}} \rangle$ because larger $\xi_{\mathbf{r}_2}$ implies more localized \mathbf{r}_2 electron and the overlapping between electron \mathbf{r}_2 with \mathbf{r}_1 is reduced, as it should be.

To evaluate \mathbf{t} one needs to know the accurate atomic orbitals [$\phi(\mathbf{r}_1, \mathbf{R})$ and $\phi(\mathbf{r}_2, \mathbf{R})$] and fortunately, IET does not require such information to predict the evolution of $\langle V_{\mathbf{R}\mathbf{R}}^{\text{sc}} \rangle$ for various doping elements. Apart from that, the two solid lines (not the arrows or dashed lines) drawn in the IET diagram (right-hand side) in Fig. 2 is the *renormalized* interaction of four solid lines in the Hubbard model diagram (left-hand side) through $\langle V_{\mathbf{R}\mathbf{R}}^{\text{sc}} \rangle$. For example, for the two-ion and two-electron system in Fig. 2, electron \tilde{e}_B screens electron \tilde{e}_A , which is attracted (Coulomb) toward ion B, and the strength of this screening depends on $\langle V_{\mathbf{R}\mathbf{R}}^{\text{sc}} \rangle$. Meaning, electron \tilde{e}_A can be thought of as an electron brought from say, infinity toward ion B,

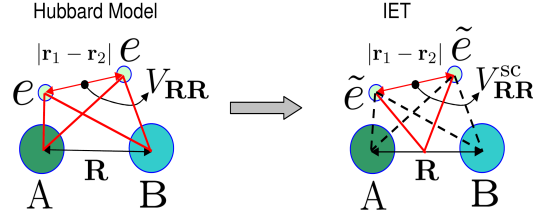


FIGURE 2. Schematic diagrams for the two-particle Hubbard model (left-hand side) and the IET version of the Hubbard model (right-hand side). A and B are two different static ions with one valence electron each. The separation between the electrons is $|\mathbf{r}_1 - \mathbf{r}_2|$, and \mathbf{R} is the separation between the ions. The effective charge, e of the electrons in the Hubbard model depends on the accurate atomic orbitals $[\phi(\mathbf{r}_1, \mathbf{R})$ and $\phi(\mathbf{r}_2, \mathbf{R})]$, while in the IET version, the effective charge, \tilde{e} is captured by the averaged screened Coulomb potential through the parameter, ξ .

and its attraction is determined by $\langle V_{sc}^{B,C} \rangle$. Here, the two solid lines are captured by $\langle V_{sc}^{B,C} \rangle$. Simply put, electron \tilde{e}_A is attracted toward ion B and screened by electron \tilde{e}_B , while at the same time, electron \tilde{e}_B is attracted toward ion A and screened by electron \tilde{e}_A , which then determine the Coulomb repulsion between electrons \tilde{e}_A and \tilde{e}_B . As a consequence, using Eq. (2.13) (from Ref. [31]), we obtain

$$(2.16) \quad \hat{V}_{sc}^A = \frac{e^2}{4\pi\epsilon_0|\mathbf{r}_1 - \mathbf{r}_2|} e^{-\mu(r_1+r_2)e^{-\frac{1}{2}\lambda(\xi_A)}} \\ : \tilde{e}_B \text{ is attracted toward A and screened by } \tilde{e}_A,$$

$$(2.17) \quad \hat{V}_{sc}^B = \frac{e^2}{4\pi\epsilon_0|\mathbf{r}_1 - \mathbf{r}_2|} e^{-\mu(r_1+r_2)e^{-\frac{1}{2}\lambda(\xi_B)}} \\ : \tilde{e}_A \text{ is attracted toward B and screened by } \tilde{e}_B.$$

Here, ξ_A and ξ_B capture the attractions between electrons A and B toward ions A and B , respectively. If $\xi_B > \xi_A$ then $\hat{V}_{sc}^B > \hat{V}_{sc}^A$, which implies that electron A is more screened (less localized) than electron B (this statement has been proven in Ref. [31] for atomic He) that eventually leads us to Fig. 3.

Figure 3(a) tells us the degree of overlapping (shaded section) between the atomic orbitals A and B . The atomic orbital, A is less localized and therefore, is widely spread as compared to the atomic orbital, B . Figure 3(b) is for the hypothetical system $AB_{1-x}C_x$. If $\xi_A < \xi_C < \xi_B$, then in average, the shaded area (degree of overlapping) increases with increasing content of ion C . Add to that, the mean positions of the shaded area should be nearer to the ion B (due to strong Coulomb attraction between electron A and ion B). Note here that, $\xi_B > \xi_A$ also implies strong Coulomb repulsion between the attracted electron A toward ion B and electron B . Therefore, in the IET framework, the Hubbard Coulomb repulsion is given by

$$(2.18) \quad U_H = \langle V_{RR}^{sc} \rangle \propto \langle \hat{V}_{sc}^A \rangle + \langle \hat{V}_{sc}^B \rangle.$$

Importantly, if for example, $\xi_A \rightarrow \infty$, $\xi_B \rightarrow \infty$ and $\xi_C \rightarrow \infty$, then the respective ion cores (A , B and C) are rigid with an effective positive charge. If on the other

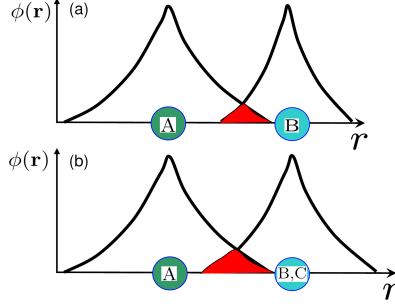


FIGURE 3. Schematic diagrams for the overlapping of atomic orbitals, A and B. (a) The shaded area, which represents the degree of overlapping depends on the relative magnitudes of ξ_A and ξ_B , where $\xi_B > \xi_A$. (b) If the conditions, $\xi_B > \xi_A$ and $\xi_C < \xi_B$ are satisfied, then the degree of overlapping for the orbitals A and (B,C) increases with the content of ion C. Here, B,C implies $B_{1-x}C_x$.

hand, $\xi_A \rightarrow 0$, $\xi_B \rightarrow 0$ and $\xi_C \rightarrow 0$, then Eq. (2.18) satisfies the Thomas-Fermi approximation (screening of free-electrons).

Unfortunately, Eq. (2.15), even though captures the evolution of the poles with changing interaction strength or energy level spacing, it is still physically identical to Eq. (2.12) in which, $U_H = 0$ also implies $\langle V_{\mathbf{R}\mathbf{R}}^{sc} \rangle = 0$ regardless whether $\xi = 0$ or $\xi \neq 0$. Therefore, we need to find an alternative way to incorporate $U_H = 0$ and $\xi \neq 0$ into the Green function. A new direction is possible if one employs the total energy eigenvalue given in the IET-Schrödinger equation [31], $H\varphi = (E_0 \pm \xi)\varphi$, to simplify the Hubbard Hamiltonian (Eq. (2.7)) such that

$$(2.19) \quad H_{\text{IET}}^H = E^{(0)} \sum_{\mathbf{R},\sigma} c_{\mathbf{R}\sigma}^\dagger c_{\mathbf{R}\sigma} + \xi \sum_{\mathbf{R}} n_{\mathbf{R}\uparrow} n_{\mathbf{R}\downarrow}.$$

Here, $E^{(0)} = E_0$ where E_0 is the total energy for 0K. The plus sign (in $\pm\xi$) is for the electrons, while the minus belongs to the holes. These signs imply that the numbers of electrons and holes are calculated in the limits 0 to ∞ (\int_0^∞) and $-\infty$ to 0 ($\int_{-\infty}^0$), respectively. Further, we have conveniently and correctly ignored the term, $\mathbf{t} \sum_{\mathbf{R}+\mathbf{d},\sigma} c_{\mathbf{R}+\mathbf{d}\sigma}^\dagger c_{\mathbf{R}\sigma}$ because \mathbf{t} is redundant within the IET formalism in which, ξ is the responsible parameter to take into account any change in the excitation or hopping probability. Having said that, we can derive the more user-friendly renormalized Green function

$$(2.20) \quad \mathcal{G}(E, \xi) = \frac{1 - \langle n_{-\sigma} \rangle}{E - E^{(0)} + i\delta} + \frac{\langle n_{-\sigma} \rangle}{E - [E^{(0)} + \xi] + i\delta}.$$

This time we have to look up the Appendix for a detailed derivation (of Eq. (2.20)) because of irritating algebra. In any case, Fig. 4 indicate the predicted density of states when $\xi \geq 0$, in which, the new condition $U_H = 0$ and $\xi \neq 0$ is actually related to Eq. (2.1), and is expected to be responsible for the strange T -linear metallic property of cuprates above T_{sc} . The full implication of Eq. (2.20) in this respect are exposed in the following Section.

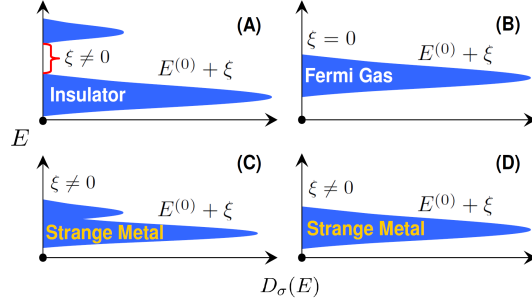


FIGURE 4. Predicted density of states, $D(\sigma, E)$ based on the atomic-limit Hubbard model within IET or Eq. (2.20). Diagram (A) depicts the usual insulating behavior similar to U_H where $\xi \neq 0$ and $U_H \neq 0$. In this case, both ξ and U_H represent the band gap. Whereas, diagram (B) shows the Fermi gas or free-electron metallic behavior because $\xi = U_H = 0$, in other words, the band overlaps due to energy-level crossings. However, strange metallic behavior is anticipated when the energy levels cross (or the energy bands overlap) in such a way that $U_H = 0$, while ξ remains finite ($\xi \neq 0$) as indicated in diagrams (C) and (D).

By now, we may have noticed that within IET, the atomic ionization energy, or the atomic energy-level spacing replaces the role of wave function (required in the Schrödinger representation), or the role of Green function in the Green function formalism. However, there is an intrinsic inadequacy within IET because it cannot be used to calculate the energy-level spacing. Instead, IET exploits the atomic energy levels to predict numerous physico-chemical-biological processes for molecules and solids via the energy-level spacing renormalization method. This means that, one still needs to make use of the Schrödinger equation or the Heisenberg representation, or the Green function formalism to calculate the energy-level spacing of any quantum system.

3. NORMAL-STATE PROPERTIES OF CUPRATE SUPERCONDUCTORS

There are numerous proposals that are available to explain the origin of T -linear property and superconductivity in solids, namely, the resonating valence bonds [33, 34, 35, 36], the pure and marginal Fermi liquid theory [37, 38, 39, 40], the non-Fermi liquid phase [41, 18, 19, 20, 42, 43], the hidden Fermi liquid with different scattering rates [44, 45, 46], and the quantum critical-point phenomenon and the Hubbard model [12, 41, 47, 48, 49, 50]. Quite recently, we also have the topological superconductors [51, 52, 53]. In this work however, we focus on IET and find out how to exploit this theory to explain the well-established experimental results self-consistently, and accurately. Recall that we will ignore the origin of (i) superconductivity, (ii) the pseudogap phenomenon, and (iii) the change of resistivity with temperature, giving rise to the T -linear effect for high T , and the approximately T^2 -effect for very low T under high magnetic fields.

We deliberately ignore the origin of T -linear effect in the normal state of superconductors, not because we are unable to provide any explanation to its existence

(in fact, we did provide in Refs. [54, 55, 56]), but because the origin of T -linear effect cannot be pinned down to a single cause. The obvious cause can be due to different scattering rates ($1/\tau_{\text{transport}} \propto T$ and $1/\tau_{\text{Hall}} \propto T^2$) as proposed in the hidden Fermi liquid theory or due to boson-boson interaction with $1/\tau_{\text{boson}} \propto T$ proposed by the gang of Philips (Philip Anderson-Philip Casey [45, 46] and Philip Phillips [47, 48], respectively). Apart from the Philips, it was Kastirnakis who had proposed a T -linear effect in cuprates (both above and below T_{sc}) entirely from the interacting Fermi liquid theory in the presence of the van Hove singularities [37, 38]. The other reason is due to the change in the valence states of multi-valent element with decreasing temperature. Changing valence states means changing ξ . Experimental proofs for this second reason were reported by Dionicio [57] using the results of Fukuda *et al.* [58], and the data points have been reproduced here in Fig. 5. Such a dependence gives rise to a T -dependent carrier density (see Eq. (3.1)), and together with different scattering rates, they influence the resistivity versus temperature curves. For example, if the carrier density, $n \propto T$, while $1/\tau_{\text{electron}} \propto T^2$, then we have the famous T -linear effect [54, 55], $\rho(T) \propto T$. Unfortunately, one also need to explain the Hall angle that is proportional to T^2 , as well as the almost temperature-independent heat conductivity [59, 60, 61] self-consistently.

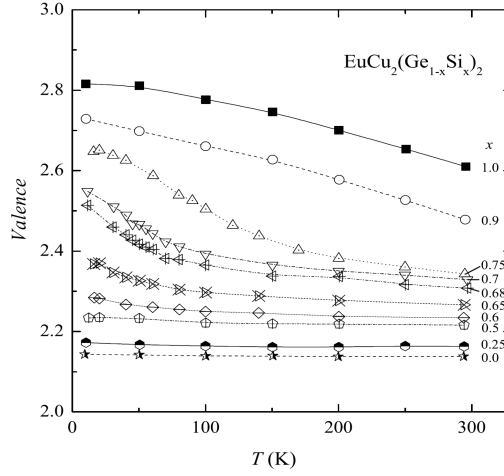


FIGURE 5. Temperature-dependent valence state of the element Eu in $\text{EuCu}_2(\text{Ge}_{1-x}\text{Si}_x)_2$ due to increasing x , which were inferred from the Eu- L_{III} edge X-ray absorption spectra obtained from Fukuda *et al.* [58]. This figure was carbon-copied from the work of Dionicio [57].

What we attempt to do here are to explain the existence of thermal assisted ^cQPT in cuprates above T_{sc} and to find out how does this continuous QPT is responsible for the existence of non-metallic (insulating), strange metallic, Fermi liquid ($g_0 > 0$) and free-electronic (Fermi gas; $g_0 = 0$) phases. Here, g_0 denotes the bare coupling constant following Ref. [3], and we will get to this point in detail later. First, we need an appropriate figure to understand the existence of these phases, and Fig. 6(A) depicts the relevant phase diagram for cuprates drawn schematically following Refs. [48, 62, 63, 64, 65, 66, 67]. Figure 6(B) shows the resistivity versus

temperature ($\rho(T)$) curves for the paths, II to V drawn in (A). The dashed lines in Fig. 6(B) show the deviations of $\rho(T)$ from the T -linear curves for paths II and III at T_{II}^* and T_{III}^* , respectively. As stated earlier, we will ignore any $\rho(T)$ curve that contain the pseudogap phase between T_{sc} and T^* because such a phase is never a prerequisite for superconductivity in cuprates.

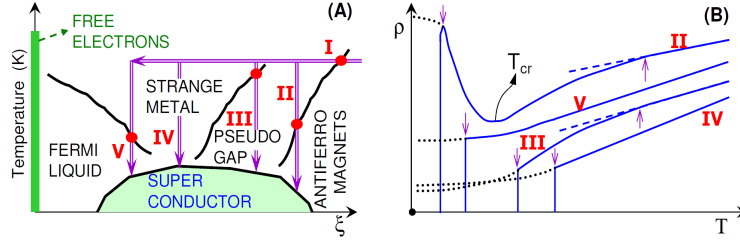


FIGURE 6. (A) Schematic phase diagram for cuprate superconductors plotted as a function of the ionization energy where the free-electron system is uniquely defined when $\xi = 0$. If one increases ξ , the system may acquire interacting Fermi liquid phase, followed by the strange-metal and pseudogap phases, before achieving the insulating antiferromagnets, through a series of electronic phase transitions at a constant temperature. (B) Resistivity (ρ) versus T curves follow the paths, II, III, IV and V as sketched in (A) in which, these schematic curves have been observed experimentally [59, 63, 64, 65, 66, 67]. All the arrows pointing downward in (B) indicate T_{sc} , while the upward arrows denote T^* . The metal-to-insulator crossover temperature is labeled as T_{cr} .

To keep the discussion straightforward, we need to exploit $\rho(T)$ curves along the paths, IV and V that may also include the metal-to-insulator crossover temperature (T_{cr}). In addition, such curves should also be presented such that T_{sc} s have been suppressed by means of magnetic fields so that the dotted lines in Fig. 6(B) can be confirmed. These dotted lines do not shoot to infinity when $T \rightarrow 0$, instead, they approach finite values that correspond to a metallic (Fermi-gas- or Fermi-liquid-like) behavior. The experimental data points satisfying paths IV and V in Fig. 6(A) are depicted in Fig. 7, which were measured by Takagi *et al.* [66], Cooper *et al.* [67] and Hussey [68]. These $\rho(T, x)$ curves are for $\text{La}_{2-x}\text{Sr}_x\text{CuO}_4$ polycrystals (A) and single crystals (B). There are two distinct electronic properties that need to be tackled self-consistently, (i) the downward shift in $\rho(T, x)$ due to increasing x and (ii) the transition to the Fermi-liquid-like metallic behavior after the T -linear effect in the absence of T_{cr} . The answer to (i) is unambiguous and self-consistent [54, 69, 70]. For example, the change in the carrier density

$$(3.1) \quad n(T, \xi) = \int_0^\infty f(E_0, \xi) D(E_0) dE = \frac{m_e^* k_B T}{\pi \hbar^2} \exp \left[\frac{-\xi_{\text{cuprate}}}{k_B T} \right],$$

is responsible for the downward shift of $\rho(T)$ with increasing x (see Fig. 7) because $\xi_{\text{Sr}^{2+}} (807 \text{ kJmol}^{-1}) < \xi_{\text{La}^{3+}} (1152 \text{ kJmol}^{-1})$. Here, ξ_{cuprate} is now the energy level spacing in $\text{La}_{2-x}\text{Sr}_x\text{CuO}_4$ determined by the content of Sr and La, hence $\xi_{\text{cuprate}} = x\xi(\text{Sr}^{2+}) + (2-x)\xi(\text{La}^{3+})$ where ξ_{cuprate} is proportional to their atomic ionization

energies of Sr^{2+} and La^{3+} . Moreover, $f(E_0, \xi)$ is the ionization energy based Fermi-Dirac statistics given in Ref. [31], $D(E_0) = m_e^*/\pi\hbar^2$ is the two-dimensional density of states, m_e^* is the electron effective mass, and E_F^0 is just a constant and we take it to be zero for convenience.

We show here that there exist a T -QPT from the strange- to Fermi-metal (with finite conductivity when $T \rightarrow 0$) within IET. Recall here that IET cannot be applied to Fermi liquid or Fermi gas because the energy-level spacing, ξ is either zero, or does not play any significant role for such systems. When one looks closely, the $\rho(T, x)$ curves in Fig. 7(A) and (B) cross each other, violating the prediction from Eq. (3.1) for different x and for $T < 100\text{K}$. The first reason that comes to mind is the T -dependent scattering rates becoming the dominant mechanism as a result of ξ now has been reduced to an insignificant constant. Note here that any Fermi liquid or Fermi gas system has the power to render ξ useless and/or redundant as it is suspected to be the case here for $T < 100\text{K}$. Nicely enough, this violation exists without significant changes occurring to ξ . For instance, when $T > 100\text{K}$, ξ very accurately determines the shift of the resistivity curves with x , however, for $T < 100\text{K}$, the effect of ξ on $\rho(T, x)$ is strangely switched-off (not because $\xi \rightarrow 0$ as $T \rightarrow 0\text{K}$). For example, the above transition for $\rho(T)$ from strange- to Fermi-metal does not require significant changes to ξ , instead ξ continuously ceases to be relevant. This means that the Fermi metal and its scattering rates become increasingly significant for $T < 100\text{K}$ without requiring $\xi \rightarrow 0$, and this conclusion somewhat points in the direction of the hidden Fermi liquid theory proposed by Anderson and Casey [45, 46], as well as the interacting Fermi liquid theory advocated by Kastrinakis [37, 38]. Unfortunately, we are unable to pin point the transition temperature between the strange- and the Fermi-metal, $T_{\text{FM}}^{\text{SM}}$ where $T_{\text{FM}}^{\text{SM}}$ is definitely not related to 100K discussed above. In fact, the value 100K is the temperature when $\rho(T, x = 0.23)$ curve crosses the curve for $\rho(T, x = 0.26)$ (see Fig. 7(B)).

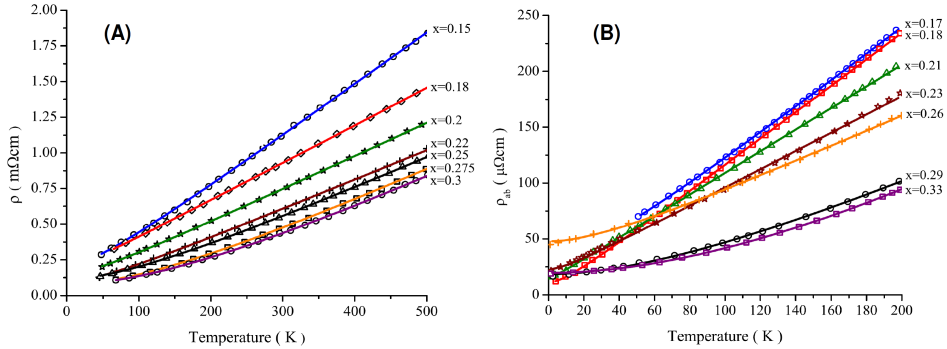


FIGURE 7. (A) The resistivity versus temperature ($\rho(T, x)$) curves for the polycrystalline $\text{La}_{2-x}\text{Sr}_x\text{CuO}_4$. (B) $\rho_{\text{ab}}(T, x)$ curves in the ab-plane (CuO_2 plane) for the $\text{La}_{2-x}\text{Sr}_x\text{CuO}_4$ single crystals measured at high magnetic fields to suppress T_{sc} . Both (A) and (B) figures were carbon-copied from Ref. [45] in which, the experimental data points were obtained from Refs. [66, 67].

Anyway, this so-called C_T QPT (from strange- to Fermi-metal) is observable in the $\rho(T, x)$ measurements (see Fig. 7(B)) because $\rho(T) \rightarrow \text{finite value}$ as $T \rightarrow 0$. Without this transition, $\rho(T) \rightarrow \infty$ as $T \rightarrow 0$ due to the existence of $\xi \neq 0$ in Eq. (3.1). This C_T QPT is actually an electronic thermal phase transition due to the existence of Eq. (2.1). For example, for a two level system, a single energy level crossing at \mathbf{k}_1 technically implies $\xi(\mathbf{k}_1) = |h_a(\mathbf{k}_1) - h_b(\mathbf{k}_1)| + |v_a(\mathbf{k}_1) - v_b(\mathbf{k}_1)| \neq 0$ where $E_a(\mathbf{k}_1) = E_b(\mathbf{k}_1)$ and $U_H = 0$ by definition. Applying this knowledge to the above problem means, for $T > T_{\text{FM}}^{\text{SM}}$, the electronic conductivity requires transport from one quantized energy level to another, which needs to overcome $\xi(\mathbf{k})$ at the points where the energy levels cross. This gives rise to the strange metallic behavior in accordance with Fig. 4(C and D). Whereas, for $T < T_{\text{FM}}^{\text{SM}}$, the same electronic transport from a quantized energy level does not cross to its neighboring energy level at the point of crossing. As such, $\xi(\mathbf{k})$ does not play a significant role below $T_{\text{FM}}^{\text{SM}}$, giving rise to the Fermi-liquid (not Fermi gas) metal, and its scattering rates are the ones that determine the temperature-dependence of $\rho(T)$. This low temperature Fermi metal is a Fermi-liquid type, rather than the Fermi-gas (free-electron) type because the latter strictly and literally requires $\xi = 0$, even though both Fermi gas and Fermi liquid have continuous network of Fermi surface. A continuous Fermi surface exists only for $\xi = 0$ and/or when $\xi \neq 0$ and $T < T_{\text{FM}}^{\text{SM}}$ where $T_{\text{FM}}^{\text{SM}}$ denotes the C_T QPT temperature between the strange- and the Fermi-metal. Any other condition does not allow a network of continuous Fermi surface independent of ξ . Apart from that, this thermal-assisted quantum phase transition includes the continuous (higher-order) thermal phase transition, and consequently, $T_{\text{FM}}^{\text{SM}}$ cannot occur at a fixed temperature, instead, it represents a temperature range without any discontinuity that can be observed indirectly in $\rho(T)$ measurements (when $\rho(T) \rightarrow \text{finite value}$ as $T \rightarrow 0\text{K}$). Therefore, we can claim here that all second- and higher-order TPT are thermal-assisted C QPT. On the other hand, the claim that all first-order TPT must go through a thermal-assisted C QPT at a constant T has been proven elsewhere [71].

There is however, one other issue that escaped our analysis thus far— the origin of T_{cr} depicted in Fig. 6(B) for path II indicates an insulating behavior just above the superconducting transition temperature. This non-metallic behavior is observable because $\xi > k_B T_{\text{cr}}$ where $\xi \neq 0$ here does not imply the existence of a band gap. In the presence of a well separated conduction and valence bands, and in the absence of any energy level crossing between them, $\xi \neq 0$ is the energy level spacing related to a band or energy gap (E_g). Therefore, for any ξ such that $\xi \neq 0$ and $E_g \neq 0$, one will always obtain an insulating system, whereas, for $\xi \neq 0$ and $E_g = 0$, one instead captures the strange metallic behavior at high temperatures, and possibly a Fermi-liquid metal at low temperatures if and only if there is a C_T QPT. The existence of Fermi liquid and strange metal for different temperature ranges implies that the emergent phenomenon put forth by Anderson [27] is actually related to QPT. In other words, indeed “more is different” but we can certainly add details to it, and claim, more interactions (not necessarily competing) within a given system will lead to different types of quantum phase transitions and emergent phases. Finally, path I in Fig. 6(B) shows the quantum phase transition due to doping or changing ξ , and in this case, the C QPT is from an antiferromagnetic insulator (large ξ) to a strange metal (low ξ) for $T > T^*$.

Having said that, we continue and complete our analysis on the normal state properties of cuprates with respect to the proof developed by the trio, Parameswaran, Shankar and Sondhi [3]. We recall the definition of Fermi-liquid based on the bare coupling constant (g_0), and the s -wave Cooper-pair frequency (Ω) derived by them. The relevant result is the two-point Cooper-pair correlation function [3],

$$(3.2) \quad \Gamma(\bar{\Omega}; g_0, \Lambda_{\text{Shankar}}) = \frac{1}{2\pi v_F} \left[\frac{a |\log(\bar{\Omega}/\Lambda_{\text{Shankar}})|}{1 + a g_0 |\log(\bar{\Omega}/\Lambda_{\text{Shankar}})|} \right],$$

where $\bar{\Omega} = (\Omega^2 + P^2)^{1/2}$, P is the s -wave Cooper-pair momentum, a denotes a positive constant, Λ_{Shankar} is the Shankar cutoff parameter, v_F denotes the Fermi velocity, and Eq. (3.2) must satisfy $\bar{\Omega} < \Lambda_{\text{Shankar}}$. For Fermi gas (free electrons), $g_0 = 0$ and for $T = 0\text{K}$, one has $\Gamma(\bar{\Omega}; g_0, \Lambda_{\text{Shankar}}) \propto |\log(\bar{\Omega}/\Lambda_{\text{Shankar}})|$, which diverges logarithmically as $\bar{\Omega} \rightarrow 0$. On the contrary, for Fermi liquid, $\Gamma(\bar{\Omega}; g_0, \Lambda_{\text{Shankar}}) \rightarrow 1/2\pi v_F g_0$, which converges to a constant as $\bar{\Omega} \rightarrow 0$. This result clearly indicate that Fermi gas is indeed a special case within the Fermi liquid formalism such that when ξ has been switched-off, one can simply take $\xi = 0$ because ξ is now an irrelevant constant. Obviously, there is a one-to-one correspondence between the Fermi gas and Fermi liquid when $\xi \rightarrow 0$, which is also in agreement with our earlier claim [62] that the Fermi gas (or a free-electron metal) has got to be an emergent phase. For example, we can write [62] $\Lambda_{\text{Shankar}} = (\hbar k^2/2m^*)\Lambda_{\text{IET}}$ and replacing Λ_{Shankar} with $(\hbar k^2/2m^*)\Lambda_{\text{IET}}$ in Eq. (3.2) does not change the above divergence or convergence in any way. In particular, for the Fermi liquid systems, $\Lambda_{\text{IET}} = \exp(\lambda\xi)$ is a constant because ξ is itself a constant, while $\lambda = (12\pi\epsilon_0/e^2)a_B$ is just a collection of constants defined earlier. As for the Fermi gas, $\Lambda_{\text{IET}} \rightarrow 1$ as $\xi \rightarrow 0$. Therefore, replacing Λ_{Shankar} with $(\hbar k^2/2m^*)\Lambda_{\text{IET}}$ within a Fermi gas or a Fermi liquid system does not change anything physically, as it should be [31, 62], except that Fermi gas is a special case exists when and only when $\xi = 0$.

4. FURTHER ANALYSIS

Contrary to our models derived earlier [21, 22, 24], the particles responsible for the strange metallic behavior discussed in this work are still electrons, but with strong correlation such that it requires $\xi \neq 0$ and ξ is not redundant. Free-electron metals simply require $\xi = 0$, while Fermi liquid embeds the condition, $\xi \neq 0$ but its magnitude is an irrelevant constant. Therefore, our strange metal is due to strongly correlated electrons requiring $\xi \neq 0$, and ξ plays an active role here such that the electron-hopping from one energy-level to another needs to overcome ξ . These energy levels are crossed for strange metals, but if they are gapped, then one obtains a semiconducting (or an insulating) normal state, however, this depends on the relationship between ξ and T . For example, one gets a metallic property if $\xi < T$, and a semiconductor otherwise.

The Green function in the atomic limit given in Eq. (2.20) is not applicable for Mott insulators. This is a false assumption. Proving it false is the main aim of this final piece. We will proceed to demonstrate why and how ξ captures the hopping of particles with different elements and elemental composition, without violating the particle-hole symmetry, without any *ad-hoc* physical interpretations. Our analyses follow Ref. [72]. We show Eq. (2.20) correctly exposes the spectral weight transfer mechanism in accordance with the data obtained from the soft X-ray absorption spectra, measured by Chen *et al.* [73]. In fact, in the atomic limit, Eq. (2.20) requires

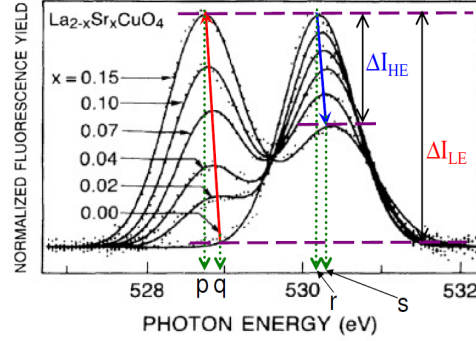


FIGURE 8. Soft X-ray absorption spectra at the oxygen-K edge for the sample, $\text{La}_{2-x}\text{Sr}_x\text{Cu}_{1-y}\text{Cu}_y^{3+}\text{O}_{4+\delta}^{2-}$ obtained by Chen *et al.* [73]. The main figure with experimental data points was carbon-copied from Ref. [73]. The intensities (I) for these peaks have been normalized, backgrounds subtracted, and the data were fitted with a Gaussian function. There are two main peaks, one being the high-energy (HE) peak (occurring between 530 and 531 eV), while the one to the left is the low-energy (LE) peak occurring slightly below 529 eV. The photon energies labeled with p and q show the red-shift (from p to q) in the LE peak for increasing x , while the blue-shift occurs from r to s in the HE peak for the same doping concentration ($0 \leq x \leq 0.15$). These shifts satisfy the inequality, $p > q > r > s$ where $q - p = \Delta_{\text{shift}}^{\text{red}}$, $s - r = \Delta_{\text{shift}}^{\text{blue}}$, $r - q = \Delta_{\text{min}}$, and $s - p = \Delta_{\text{max}}$. Here, $\Delta_{\text{shift}}^{\text{red}}$ and $\Delta_{\text{shift}}^{\text{blue}}$ denote the total red and blue shifts for the stated doping levels, while Δ_{min} and Δ_{max} are the minimum and maximum changes to the electrons energy levels, again within the investigated doping range. The change in the normalized intensities for the high- and low-energy sectors are denoted by ΔI_{HE} and ΔI_{LE} , respectively.

one to write $\xi = \xi_{\text{systems}}^{\text{atomic}}$, for molecules, one has $\xi_{\text{systems}}^{\text{molecular}}$, and for a specific solid, namely, for cuprates one writes ξ_{cuprates} . Hence, the many-body problem here is to calculate the many-body energy level spacing denoted by $\xi_{\text{body}}^{\text{many}}$. For atomic systems, ξ is known almost exactly since we can obtain it from the atomic spectra, whereas, for other compounds and molecules, we need to invoke the ionization energy approximation [54], which states, the energy level spacing of a compound is proportional to the energy level spacings of the compound's constituent atoms. For example, the energy level spacing for a hypothetical compound, $\text{AB}_{1-x}\text{C}_x$ is given by $\xi_{\text{AB}_{1-x}\text{C}_x} = x\xi_{\text{C}} + (1-x)\xi_{\text{B}}$ (see Fig. 3(b)). In this case, we can exclude the contribution from A because ξ_{A} is a constant anyway.

We now recall the soft X-ray absorption spectra measured by Chen *et al.* [73] depicted in Fig. 8. These spectra correspond to the changes in the concentrations of Sr^{2+} , La^{3+} , Cu^{2+} , Cu^{3+} and O^{2-} in the compound, $\text{La}_{2-x}\text{Sr}_x\text{Cu}_{1-y}\text{Cu}_y^{3+}\text{O}_{4+\delta}^{2-}$. Unlike the simplified hypothetical $\text{AB}_{1-x}\text{C}_x$ system discussed earlier (the concentration of A is made to be constant), doping Sr^{2+} into $\text{La}_2\text{Cu}_{1-y}\text{Cu}_y^{3+}\text{O}_{4.005}^{2-}$ gives rise to changing δ and y , which have been discussed in detail elsewhere for other

oxides and multi-element solids [70, 74, 75, 76]. For example, such changes are due to defects, types of defects and the required overall charge neutrality in the system. In particular, since $\delta = 0.005$, we need $y = 0.01/3$ for charge neutrality. In the presence of Sr ($0 \leq x \leq 0.15$), both y and δ can, and will change, satisfying the linear equation, $x - y - 8 = 2\delta$ where $\{x, y\} \in [0, 1]$ and $\delta \in [0, \frac{1}{2}]$. This knowledge will become handy shortly.

Now, one can immediately observe four interesting features in the spectra plotted in Fig. 8. The first being p and q for $x > 0$ appear at energies lower than r and s where $p = q = 0$ if $x = 0$ (undoped sample). Second, the normalized intensities, I_{LE} increases, while I_{HE} decreases with x . Third, the red ($\Delta_{\text{shift}}^{\text{red}}$) and blue ($\Delta_{\text{shift}}^{\text{blue}}$) shifts appear for the low- and high-energy peaks, respectively, with increasing x , and finally there are some asymmetric changes to the normalized intensities for the range $0 \leq x \leq 0.15$, such that $\Delta I_{LE} > \Delta I_{HE}$ (see Fig. 8). In other words, I_{LE} increases faster than $|dI_{HE}/dx|$.

The answer to the first feature is straightforward, it is due to the fact that $\xi_{\text{Sr}^{2+}}$ (807 kJmol^{-1}) $<$ $\xi_{\text{La}^{3+}}$ (1152 kJmol^{-1}). This means that the electrons with low ionization energies (from Sr^{2+}) need low photon energies to be excited, compared to the electrons with large ionization energies (from La^{3+}). Here, all ionization energy values were averaged following Ref. [54], while the values before averaging were obtained from Ref. [77]. The second feature is also obvious, the change in the normalized intensities are due to increasing x and decreasing $2 - x$ for the low- and high-energy sectors, respectively.

The red and blue shifts in the spectral weight transfer are also depicted in Fig. 8 with appropriate arrows. Understandably, the red-shift originates from the concentration of Sr^{2+} , or due to increasing x . This implies that more electrons from Sr^{2+} are needed to establish this LE peak at the lowest possible energy as a result of $\xi_{\text{Sr}^{2+}} < \xi_{\text{La}^{3+}}$. Recall that IET requires electrons with the lowest atomic ionization energies to form the valence electrons in a non-Fermi gas compound containing that particular atom. These (valence) electrons also interact weakly with the core electrons (coming from La and Cu), giving rise to smaller energy level spacings. The core electrons form large energy level spacings due to strong interaction among the core electrons [31]. As a consequence, the HE peak corresponds to the core electrons (due to large ionization energy) coming from La_{2-x}^{3+} . These core electrons interact more strongly with other core electrons coming from Cu_{1-y}^{2+} and Cu_y^{3+} ($\xi_{\text{Cu}^{2+}} = 1352 \text{ kJmol}^{-1}$ and $\xi_{\text{Cu}^{3+}} = 2086 \text{ kJmol}^{-1}$) giving rise to HE peak. This strong electron-electron interaction also explains why the energy distribution can and will spread from low to high energies as a result of the interaction among the core electrons and between the valence and core electrons.

We know from the above discussion that increasing x causes y to increase to maintain charge neutrality, and therefore, the decreasing number of large ionization energy electrons from La_{2-x}^{3+} are systematically being compensated by the large ionization energy electrons from Cu^{3+} (due to increasing y). This scenario is further enhanced if δ is also found to increase with increasing x . Therefore, we can now see the reason why HE peak blue shifts and $\Delta I_{LE} > \Delta I_{HE}$; they are due to increasing y , $2 - x \geq 1$ and/or increasing δ . For example, in the absence of this compensation effect, the HE peak should red shift with decreasing $2 - x$. But this is not the case, made sure by increasing y , and the peak will not disappear even when $x = 1$ because $2 - x \neq 0$ and $y \propto x$. Note here that we did not assume La^{3+} contribute

three electrons, while each Sr^{2+} gives two electrons. As a matter of fact, the carrier density increases with increasing Sr^{2+} in accordance with Eq. (3.1). Therefore, the compensation effect slows down I_{HE} from decreasing faster than the increasing I_{LE} , and therefore $\Delta I_{\text{LE}} > \Delta I_{\text{HE}}$. Indeed, the blue-shift is due to $\xi_{\text{Cu}^{2+,3+}}$ (1352, 2086 kJmol^{-1}) $>$ $\xi_{\text{La}^{3+}}$ (1152 kJmol^{-1}). In summary, we did not encounter any tragedy between IET Green function and the spectral weight transfer measurements, including the observed doping-dependent spectral red and blue shifts in the so-called La-Sr-Cu-O Mott insulator.

5. CONCLUSIONS

Our primary objective is to prove the existence of a thermal-assisted quantum phase transition between a strange- and a Fermi-metal in cuprates. To achieve this, we have first developed the proof where an electronic phase transition occurring in the normal state of cuprates is a type of C_T QPT. This transition is exposed to exist in cuprates above the superconducting transition temperature, when the temperature is lowered in the presence of high magnetic fields, using the Green function formalism. Using the renormalized Green function, and by requiring (i) zero energy gap, (ii) non-zero energy level crossings, and (iii) non-zero energy-level spacings, we obtained the strange metallic phase with its resistivity curve shifts accordingly with respect to changing energy-level spacing or doping. At a lower temperature however, there is this C_T QPT, which is responsible for the strange- to the Fermi-metal transition as a result of insignificant effect from the energy-level spacing because it is being switched-off continuously with lowering temperature at the points where the energy levels cross.

Along the way, the proof developed by Parameswaran, Shankar and Sondhi is coupled to the ionization energy theory to show that indeed Fermi gas is a special case within the energy-level spacing renormalization group method because Fermi gas can only exist if the energy-level spacing is zero, while the original condition that requires infinite energy-level crossings is actually necessary, but not sufficient for this phase (Fermi gas) to exist.

Finally, we demonstrated why and how the spectral weight transfer occurs for different doping elements and concentrations, including the red and blue shifting effects, and the asymmetric changes to the normalized intensities between the low- and high-energy peaks. We found all the features observed in the soft X-ray spectra for the La-Sr-Cu-O system have been captured self-consistently. These spectra, and their red and blue shifts nicely correspond to the changes in the ionization energies for different doping elements and concentrations.

It would be interesting if we could find ways to exploit this energy-level spacing such that it can be associated to the origin of superconductivity and the pseudogap phase, which have been excluded systematically for convenience, but this is another story for another day.

ACKNOWLEDGMENTS

This work was supported by Sebastiammal Innasimuthu and Arulsamy Innasimuthu. I am grateful to Amelia Das Anthony, Malcolm Anandraj and Kingston Kisshenraj for their kind and continuous hospitality. Part of this work, and the Appendix were completed while I was with the Condensed Matter Group, Division of Mathematics and Physics, Glebe, Sydney, Australia, between Aug/2009 and Feb/2010, hosted

by the late Madam Kithriammal Soosay. Special thanks to an anonymous reader for directing me to Refs. [37, 38].

6. APPENDIX: DERIVATION OF EQ. (2.20)

We start from Eq. (2.2)

$$\begin{aligned} \mathcal{G}(t-t') &= -\frac{i}{\hbar}\theta(t-t')\langle\{c_\alpha(t), c_\alpha^\dagger(t')\}\rangle \\ &= -\frac{i}{\hbar}\theta(t-t')\langle c_\alpha(t)c_\alpha^\dagger(t') + c_\alpha^\dagger(t')c_\alpha(t)\rangle. \end{aligned} \quad (6.1)$$

Subsequently,

$$\begin{aligned} \frac{\partial \mathcal{G}(t-t')}{\partial t} &= -\frac{i}{\hbar}\frac{\partial \theta(t-t')}{\partial t}\langle c_\alpha(t)c_\alpha^\dagger(t')\rangle - \frac{i}{\hbar}\theta(t-t')\left\langle \frac{\partial c_\alpha(t)}{\partial t}c_\alpha^\dagger(t') \right\rangle \\ &\quad - \frac{i}{\hbar}\frac{\partial \theta(t-t')}{\partial t}\langle c_\alpha^\dagger(t')c_\alpha(t)\rangle - \frac{i}{\hbar}\theta(t-t')\left\langle c_\alpha^\dagger(t')\frac{\partial c_\alpha(t)}{\partial t} \right\rangle. \end{aligned} \quad (6.2)$$

Noting Eq. (2.3) and after some algebraic rearrangements,

$$i\hbar\frac{\partial \mathcal{G}(t-t')}{\partial t} = \delta(t-t')\langle\{c_\alpha(t), c_\alpha^\dagger(t')\}\rangle - \frac{i}{\hbar}\theta(t-t')\left\langle \left\{ i\hbar\frac{\partial c_\alpha(t)}{\partial t}, c_\alpha^\dagger(t') \right\} \right\rangle. \quad (6.3)$$

Now, the expectation value of operator c_α at time t_1 is

$$\langle c_\alpha(t) \rangle = \langle \varphi(t) | c_\alpha(t_1) | \varphi(t) \rangle. \quad (6.4)$$

The equation of motion with respect to a constant $c_\alpha(t_1)$ is

$$i\hbar\frac{\partial \langle c_\alpha(t) \rangle}{\partial t} = \left(i\hbar\frac{\partial \langle \varphi(t) |}{\partial t} \right) c_\alpha(t_1) | \varphi(t) \rangle + \langle \varphi(t) | c_\alpha(t_1) \left(i\hbar\frac{\partial | \varphi(t) \rangle}{\partial t} \right), \quad (6.5)$$

where $\varphi(t)$ is some time-dependent wave function and therefore, $|\varphi(t)\rangle$ is the state vector. The complex conjugation requires, $(i\hbar\partial\langle\varphi(t)|)/\partial t = \langle\varphi(t)|(-H)$, thus

$$\begin{aligned} i\hbar\frac{\partial \langle c_\alpha(t) \rangle}{\partial t} &= \langle \varphi(t) | (-H)c_\alpha(t_1) | \varphi(t) \rangle + \langle \varphi(t) | c_\alpha(t_1) H | \varphi(t) \rangle \\ &= \langle \varphi(t) | [c_\alpha(t_1), H] | \varphi(t) \rangle. \end{aligned} \quad (6.6)$$

We now replace the dummy time label t_1 with t and substitute Eq. (6.6) into Eq. (6.3) to obtain

$$i\hbar\frac{\partial \mathcal{G}(t-t')}{\partial t} = 1 - \frac{i}{\hbar}\theta(t-t')\left\langle \left\{ [c_\alpha(t), H], c_\alpha^\dagger(t') \right\} \right\rangle, \quad (6.7)$$

where $H = H_{\text{IET}}^{\text{H}}$ from Eq. (2.19), and $\{c_{j\sigma}(t), c_{j\sigma}^\dagger(t')\} = 1$ because $\delta(t-t') = 1$. We move on by first evaluating

$$\begin{aligned} [c_\alpha(t), H_{\text{IET}}^{\text{H}}] &= c_{i\sigma}(E^{(0)}c_{j\sigma'}^\dagger c_{j\sigma'} + \xi c_{j\sigma'}^\dagger c_{j\sigma'} c_{j-\sigma'}^\dagger c_{j-\sigma'}) \\ &\quad - (E^{(0)}c_{j\sigma'}^\dagger c_{j\sigma'} + \xi c_{j\sigma'}^\dagger c_{j\sigma'} c_{j-\sigma'}^\dagger c_{j-\sigma'}) c_{i\sigma} \\ &= E^{(0)}(c_{i\sigma} c_{j\sigma'}^\dagger c_{j\sigma'} - c_{j\sigma'}^\dagger c_{j\sigma'} c_{i\sigma}) \\ &\quad + \xi(c_{i\sigma} c_{j\sigma'}^\dagger c_{j\sigma'} c_{j-\sigma'}^\dagger c_{j-\sigma'} - c_{j\sigma'}^\dagger c_{j\sigma'} c_{j-\sigma'}^\dagger c_{j-\sigma'} c_{i\sigma}), \end{aligned} \quad (6.8)$$

where i and j are dummy indices (dummies for short) replacing \mathbf{R} , while the spin dummies, σ' and $-\sigma'$ denote spin-up and down, respectively, however, the dummy, σ can either be spin-up or down. All the annihilation and creation operators are summed over and these dummies are necessary to keep track of these operators

when they operate from left to right or vice versa. The term with $E^{(0)}$ on the right-hand side (RHS) of Eq. (6.8) is

$$\begin{aligned} E^{(0)}(c_{i\sigma}c_{j\sigma'}^\dagger c_{j\sigma'} - c_{j\sigma'}^\dagger c_{j\sigma'} c_{i\sigma}) &= E^{(0)}((1 - c_{j\sigma'}^\dagger c_{i\sigma})c_{j\sigma'} - c_{j\sigma'}^\dagger c_{j\sigma'} c_{i\sigma}) \\ (6.9) \quad &= E^{(0)}(c_{j\sigma'} + c_{j\sigma'}^\dagger c_{j\sigma'} c_{i\sigma} - c_{j\sigma'}^\dagger c_{j\sigma'} c_{i\sigma})\delta_{ij}\delta_{\sigma'\sigma} = E^{(0)}c_{i\sigma}. \end{aligned}$$

The first term with ξ on the RHS of Eq. (6.8) is

$$\begin{aligned} \xi(c_{i\sigma}c_{j\sigma'}^\dagger c_{j\sigma'} c_{j-\sigma'}^\dagger c_{j-\sigma'}) &= \xi((1 - c_{j\sigma'}^\dagger c_{i\sigma})c_{j\sigma'} c_{j-\sigma'}^\dagger c_{j-\sigma'}) \\ &= \xi(c_{j\sigma'} c_{j-\sigma'}^\dagger c_{j-\sigma'} - c_{j\sigma'}^\dagger c_{i\sigma} c_{j\sigma'} c_{j-\sigma'}^\dagger c_{j-\sigma'}) \\ &= \xi(c_{j\sigma'} c_{j-\sigma'}^\dagger c_{j-\sigma'} \delta_{ij}\delta_{\sigma\sigma'} + c_{j\sigma'}^\dagger c_{j\sigma'} c_{j-\sigma'} \delta_{ij}\delta_{\sigma\sigma'} \delta_{\sigma-\sigma'} \\ (6.10) \quad &+ c_{j\sigma'}^\dagger c_{j\sigma'} c_{j-\sigma'}^\dagger c_{j-\sigma'} c_{i\sigma}). \end{aligned}$$

The above and all the similar evaluations follow the fermionic-operator rules, for example, $c_{i\sigma}c_{j\sigma'}^\dagger = 1 - c_{j\sigma'}^\dagger c_{i\sigma}$, $c_{i\sigma}c_{j\sigma'} = -c_{j\sigma'} c_{i\sigma}$, $n_{j\sigma'} = c_{j\sigma'}^\dagger c_{j\sigma'}$ and $n_{j-\sigma'} c_{j\sigma'} = c_{j\sigma'} n_{j-\sigma'}$. Anyway, the last term in Eq. (6.8) is nothing but the last term on the RHS of Eq. (6.10). Therefore,

$$\begin{aligned} \xi(c_{i\sigma}c_{j\sigma'}^\dagger c_{j\sigma'} c_{j-\sigma'}^\dagger c_{j-\sigma'} - c_{j\sigma'}^\dagger c_{j\sigma'} c_{j-\sigma'}^\dagger c_{j-\sigma'} c_{i\sigma}) \\ = \xi(c_{j\sigma'} n_{j-\sigma'} \delta_{ij}\delta_{\sigma\sigma'} + n_{j\sigma'} c_{j-\sigma'} \delta_{ij}\delta_{\sigma\sigma'} \delta_{\sigma-\sigma'}) \\ (6.11) \quad = \xi(n_{i-\sigma} c_{i\sigma} + n_{i\sigma} c_{i\sigma}) = \xi n_{i-\sigma} c_{i\sigma}. \end{aligned}$$

In the last step, we have replaced the dummies, j , $-\sigma'$ and σ' with i , $-\sigma$ and σ , accordingly via the Kronecker deltas and $n_{i\sigma} c_{i\sigma} = c_{i\sigma}^\dagger c_{i\sigma} c_{i\sigma} = 0$. When the above creation and annihilation operators operate from left to right or vice versa, two Kronecker deltas pop out in response for each operation, one for the lattice sites and the other for spins. We can now write (after replacing α with dummies, j and σ)

$$\begin{aligned} i\hbar \frac{\partial \mathcal{G}(t-t')}{\partial t} &= 1 - \frac{i}{\hbar} \theta(t-t') \langle \{ (E^{(0)} c_{i\sigma} + \xi n_{i-\sigma} c_{i\sigma}), c_{j\sigma}^\dagger(t') \} \rangle \\ &= 1 - E^{(0)} \frac{i}{\hbar} \theta(t-t') \langle \{ c_{i\sigma}(t), c_{j\sigma}^\dagger(t') \} \rangle \\ (6.12) \quad &- \xi \frac{i}{\hbar} \theta(t-t') \langle \{ n_{i-\sigma} c_{i\sigma}(t), c_{j\sigma}^\dagger(t') \} \rangle. \end{aligned}$$

Using Eq. (6.1) we can rewrite Eq. (6.12)

$$(6.13) \quad \left[i\hbar \frac{\partial}{\partial t} - E^{(0)} \right] \mathcal{G}(t-t') = 1 + \xi \mathcal{G}^{(1)}(t-t').$$

Note here the new substitution

$$(6.14) \quad \mathcal{G}^{(1)}(t-t') = -\frac{i}{\hbar} \theta(t-t') \langle \{ n_{i-\sigma} c_{i\sigma}(t), c_{j\sigma}^\dagger(t') \} \rangle,$$

which needs to be evaluated in the form of

$$\begin{aligned} i\hbar \frac{\partial \mathcal{G}^{(1)}(t-t')}{\partial t} &= \delta(t-t') \langle \{ n_{i-\sigma} c_{i\sigma}(t), c_{j\sigma}^\dagger(t') \} \rangle \\ (6.15) \quad &- \frac{i}{\hbar} \theta(t-t') \left\langle \left\{ n_{i-\sigma} i\hbar \frac{\partial c_{i\sigma}(t)}{\partial t}, c_{j\sigma}^\dagger(t') \right\} \right\rangle. \end{aligned}$$

We have dropped ξ from Eq. (6.15) for the time being. Now, since $\delta(t-t') = 1$, one can then employ the fermionic rule, $\{c_{i\sigma}(t), c_{j\sigma}^\dagger(t')\} = \{c_{i\sigma}, c_{j\sigma}^\dagger\} = 1$ and Eq. (6.6) to obtain

$$(6.16) \quad i\hbar \frac{\partial \mathcal{G}^{(1)}(t-t')}{\partial t} = \langle n_{i-\sigma} \rangle - \frac{i}{\hbar} \theta(t-t') \left\langle \left\{ [n_{i-\sigma} c_{i\sigma}(t), H_{\text{IET}}^{\text{H}}], c_{j\sigma}^\dagger(t') \right\} \right\rangle.$$

The next obvious step is to evaluate

$$(6.17) \quad \begin{aligned} [n_{i-\sigma} c_{i\sigma}(t), H_{\text{IET}}^{\text{H}}] &= n_{i-\sigma} c_{i\sigma} (E^{(0)} c_{j\sigma'}^\dagger c_{j\sigma'} + \xi c_{j\sigma'}^\dagger c_{j\sigma'} c_{j-\sigma'}^\dagger c_{j-\sigma'}) \\ &\quad - (E^{(0)} c_{j\sigma'}^\dagger c_{j\sigma'} + \xi c_{j\sigma'}^\dagger c_{j\sigma'} c_{j-\sigma'}^\dagger c_{j-\sigma'}) n_{i-\sigma} c_{i\sigma} \\ &= E^{(0)} (n_{i-\sigma} c_{i\sigma} c_{j\sigma'}^\dagger c_{j\sigma'} - c_{j\sigma'}^\dagger c_{j\sigma'} n_{i-\sigma} c_{i\sigma}) \\ &\quad + \xi (n_{i-\sigma} c_{i\sigma} c_{j\sigma'}^\dagger c_{j\sigma'} c_{j-\sigma'}^\dagger c_{j-\sigma'} - c_{j\sigma'}^\dagger c_{j\sigma'} c_{j-\sigma'}^\dagger c_{j-\sigma'} n_{i-\sigma} c_{i\sigma}). \end{aligned}$$

We first evaluate the term with $E^{(0)}$ from Eq. (6.17)

$$(6.18) \quad \begin{aligned} &E^{(0)} n_{i-\sigma} \left[c_{i\sigma} c_{j\sigma'}^\dagger c_{j\sigma'} - c_{j\sigma'}^\dagger c_{j\sigma'} c_{i\sigma} \right] \\ &= E^{(0)} n_{i-\sigma} \left[(1 - c_{j\sigma'}^\dagger c_{i\sigma}) c_{j\sigma'} - c_{j\sigma'}^\dagger c_{j\sigma'} c_{i\sigma} \right] \\ &E^{(0)} n_{i-\sigma} \left[c_{j\sigma'} + c_{j\sigma'}^\dagger c_{j\sigma'} c_{i\sigma} - c_{j\sigma'}^\dagger c_{j\sigma'} c_{i\sigma} \right] \delta_{ij} \delta_{\sigma\sigma'} = E^{(0)} n_{i-\sigma} c_{i\sigma}. \end{aligned}$$

The term with ξ from Eq. (6.17) is

$$(6.19) \quad \begin{aligned} &\xi \left[n_{i-\sigma} c_{i\sigma} c_{j\sigma'}^\dagger c_{j\sigma'} c_{j-\sigma'}^\dagger c_{j-\sigma'} - c_{j\sigma'}^\dagger c_{j\sigma'} c_{j-\sigma'}^\dagger c_{j-\sigma'} n_{i-\sigma} c_{i\sigma} \right] \\ &= \xi n_{i-\sigma} \left[c_{i\sigma} c_{j\sigma'}^\dagger c_{j\sigma'} c_{j-\sigma'}^\dagger c_{j-\sigma'} - c_{j\sigma'}^\dagger c_{j\sigma'} c_{j-\sigma'}^\dagger c_{j-\sigma'} c_{i\sigma} \right] \\ &= \xi n_{i-\sigma} \left[c_{j\sigma'} c_{j-\sigma'}^\dagger c_{j-\sigma'} + c_{j\sigma'}^\dagger c_{j\sigma'} c_{j-\sigma'} + c_{j\sigma'}^\dagger c_{j\sigma'} c_{j-\sigma'}^\dagger c_{j-\sigma'} c_{i\sigma} \right. \\ &\quad \left. - c_{j\sigma'}^\dagger c_{j\sigma'} c_{j-\sigma'}^\dagger c_{j-\sigma'} c_{i\sigma} \right] \\ &= \xi n_{i-\sigma} \left[c_{j\sigma'} c_{j-\sigma'}^\dagger c_{j-\sigma'} \delta_{ij} \delta_{\sigma\sigma'} + c_{j\sigma'}^\dagger c_{j\sigma'} c_{j-\sigma'} \delta_{ij} \delta_{\sigma\sigma'} \delta_{\sigma-\sigma'} \right] \\ &= \xi n_{i-\sigma} \left[c_{i\sigma} c_{i-\sigma}^\dagger c_{i-\sigma} + c_{i\sigma}^\dagger c_{i\sigma} c_{i\sigma} \right] \\ &= \xi n_{i-\sigma} c_{i\sigma}, \end{aligned}$$

again the Kronecker deltas took care of the dummies, $(c_{i\sigma})^2 = 0$ and

$$(6.20) \quad \begin{aligned} n_{i-\sigma}^2 &= c_{i-\sigma}^\dagger c_{i-\sigma} c_{i-\sigma}^\dagger c_{i-\sigma} = c_{i-\sigma}^\dagger (1 - c_{i-\sigma}^\dagger c_{i-\sigma}) c_{i-\sigma} \\ &= c_{i-\sigma}^\dagger c_{i-\sigma} - c_{i-\sigma}^\dagger c_{i-\sigma}^\dagger c_{i-\sigma} c_{i-\sigma} = n_{i-\sigma}. \end{aligned}$$

Therefore

$$(6.21) \quad [n_{i-\sigma} c_{i\sigma}(t), H_{\text{IET}}^{\text{H}}] = \xi n_{i-\sigma} c_{i\sigma}(t) + E^{(0)} n_{i-\sigma} c_{i\sigma}(t),$$

and after substituting Eq. (6.21) into Eq. (6.16)

$$\begin{aligned}
i\hbar \frac{\partial \mathcal{G}^{(1)}(t-t')}{\partial t} &= \langle n_{i-\sigma} \rangle - \frac{i}{\hbar} \theta(t-t') \left\langle \left\{ [n_{i-\sigma} c_{i\sigma}(t), H_{\text{IET}}^{\text{H}}], c_{j\sigma}^{\dagger}(t') \right\} \right\rangle \\
&= \langle n_{i-\sigma} \rangle - \xi \frac{i}{\hbar} \theta(t-t') \left\langle \left\{ [n_{i-\sigma} c_{i\sigma}(t), c_{j\sigma}^{\dagger}(t')] \right\} \right\rangle \\
(6.22) \quad -E^{(0)} \frac{i}{\hbar} \theta(t-t') &\left\langle \left\{ [n_{i-\sigma} c_{i\sigma}(t), c_{j\sigma}^{\dagger}(t')] \right\} \right\rangle.
\end{aligned}$$

Using Eq. (6.14) one can simplify Eq. (6.22)

$$\begin{aligned}
i\hbar \frac{\partial \mathcal{G}^{(1)}(t-t')}{\partial t} &= \langle n_{i-\sigma} \rangle + \xi \mathcal{G}^{(1)}(t-t') + E^{(0)} \mathcal{G}^{(1)}(t-t'), \\
(6.23) \quad \left[i\hbar \frac{\partial}{\partial t} - E^{(0)} - \xi \right] \mathcal{G}^{(1)}(t-t') &= \langle n_{i-\sigma} \rangle.
\end{aligned}$$

Subsequently, one obtains (after using the correspondence rule, $i\hbar \partial/\partial t \rightarrow E$)

$$(6.24) \quad \mathcal{G}^{(1)}(t-t') = \frac{\langle n_{i-\sigma} \rangle}{E - E^{(0)} - \xi}.$$

We substitute Eq. (6.24) back into Eq. (6.13) to arrive at our final destination

$$\begin{aligned}
(E - E^{(0)}) \mathcal{G}(t-t') &= 1 + \frac{\xi \langle n_{i-\sigma} \rangle}{E - E^{(0)} - \xi}. \\
(E - E^{(0)}) \mathcal{G}(t-t') &= \frac{E - E^{(0)} - \xi}{E - E^{(0)} - \xi} + \frac{\xi \langle n_{i-\sigma} \rangle}{E - E^{(0)} - \xi}. \\
(E - E^{(0)}) (E - E^{(0)} - \xi) \mathcal{G}(t-t') &= E - E^{(0)} - \xi + \xi \langle n_{i-\sigma} \rangle \\
&= E \langle n_{i-\sigma} \rangle - E \langle n_{i-\sigma} \rangle + E^{(0)} \langle n_{i-\sigma} \rangle - E^{(0)} \langle n_{i-\sigma} \rangle + E - E^{(0)} - \xi + \xi \langle n_{i-\sigma} \rangle \\
&= (E - E^{(0)}) \langle n_{i-\sigma} \rangle - \langle n_{i-\sigma} \rangle (E - E^{(0)} - \xi) + E - E^{(0)} - \xi.
\end{aligned}$$

Therefore

$$(6.25) \quad \mathcal{G}(t-t') = \frac{\langle n_{i-\sigma} \rangle}{E - (E^{(0)} + \xi) + i\delta} + \frac{1 - \langle n_{i-\sigma} \rangle}{E - E^{(0)} + i\delta},$$

after introducing the arbitrary convergence factor, δ .

REFERENCES

- [1] J. G. Bednorz, K. A. Müller, Z. Phys. B **64**, 189 (1986).
- [2] P. W. Anderson, *The Theory of Superconductivity in the High- T_c Cuprates*, (Princeton University Press, Princeton, 1995, USA).
- [3] S. A. Parameswaran, R. Shankar, S. L. Sondhi, Phys. Rev. B **82**, 195104 (2010).
- [4] L. D. Landau, Sov. Phys. JETP **3**, 920 (1957).
- [5] L. D. Landau, Sov. Phys. JETP **5**, 101 (1957).
- [6] L. D. Landau, Sov. Phys. JETP **8**, 70 (1959).
- [7] A. A. Abrikosov, L. P. Gorkov, I. E. Dzyaloshinski, *Methods of Quantum Field Theory in Statistical Physics*, (Prentice-Hall, Inc., New Jersey, 1963, USA).
- [8] N. W. Ashcroft, N. D. Mermin, *Solid State Physics*, (Holt, Rinehart, and Winston, N.Y., 1976, USA).
- [9] T. Senthil, Ann. Phys. (N.Y.) **321**, 1669 (2006).
- [10] J. Simon, W. S. Bakr, R. Ma, M. E. Tai, P. M. Preiss, M. Greiner, Nature **472**, 307 (2011).
- [11] S. Sachdev, Ann. Phys. (N.Y.) **303**, 226 (2003).
- [12] S. Sachdev, Phys. Status Solidi B **247**, 537 (2010).
- [13] S. Sachdev, X. Yin, Ann. Phys. (N.Y.) **325**, 2 (2010).

- [14] L. Balents, S. Sachdev, Ann. Phys. (N.Y.) **322**, 2635 (2007).
- [15] T. Senthil, R. Shankar, Phys. Rev. Lett. **102**, 046406 (2009).
- [16] J. Hubbard, Proc. R. Soc. A **276**, 238 (1963).
- [17] N. F. Mott, Rev. Mod. Phys. **40**, 677 (1968).
- [18] I. Ichinose, T. Matsui, M. Onoda, Phys. Rev. B **64**, 104516 (2001).
- [19] M. Onoda, I. Ichinose, T. Matsui, J. Phys. Soc. Jpn. **61**, 2606 (1998).
- [20] M. Onoda, I. Ichinose, T. Matsui, J. Phys. Soc. Jpn. **69**, 3497 (2000).
- [21] A. D. Arulsamy, P. C. Ong, M. T. Ong, Physica B **325**, 164 (2003).
- [22] A. D. Arulsamy, Physica B **352**, 285 (2004).
- [23] L. B. Ioffe, A. I. Larkin, Phys. Rev. B **39**, 8988 (1989).
- [24] A. D. Arulsamy, Physica C **420**, 95 (2005).
- [25] N. Mannella, W. L. Wang, X. J. Zhou, H. Zheng, J. F. Mitchell, J. Zaanen, T. P. Devereaux, N. Nagaosa, Z. Hussain, Z. X. Shen, Nature **438**, 474 (2005).
- [26] A. D. Arulsamy, Prog. Theor. Phys. **126**, article in press (2011).
- [27] P. W. Anderson, Science **177**, 393 (1972).
- [28] U. Rössler, *Solid State Theory* (Springer-Verlag, Berlin, 2004, Germany).
- [29] G. D. Mahan, *Many-Particle Physics*, (Plenum, N.Y., 1981, USA).
- [30] J. M. Ziman, *Elements of Advanced Quantum Theory*, (Cambridge University Press, 1969, UK).
- [31] A. D. Arulsamy, Pramana J. Phys. **74**, 615 (2010); A. D. Arulsamy, PhD thesis, The University of Sydney, Australia (2009).
- [32] R. Shankar, Rev. Mod. Phys. **66**, 129 (1994).
- [33] G. Baskaran, Z. Zou, P. W. Anderson, Solid State Commun. **63**, 973 (1987).
- [34] G. Baskaran, Pramana J. Phys. **73**, 61 (2009).
- [35] G. Baskaran, J. Phys. Soc. Jpn. **77**, 113713 (2008).
- [36] G. Baskaran, Ind. J. Phys. **80**, 583 (2006).
- [37] G. Kastinakis, Physica C **340**, 119 (2000).
- [38] G. Kastinakis, Phys. Rev. B **71**, 014520 (2005).
- [39] C. M. Varma, P. B. Littlewood, S. Schmitt-Rink, E. Abrahams, A. E. Ruckenstein, Phys. Rev. Lett. **63**, 1996 (1989).
- [40] C. M. Varma, Z. Nussinov, W. van Saarloos, Phys. Rep. **361**, 267 (2002).
- [41] T. Senthil, Phys. Rev. B **78**, 035103 (2008).
- [42] P. A. Lee, Physica C **317**, 194 (1999).
- [43] P. A. Lee, N. Nagaosa, Phys. Rev. B **46**, 5621 (1992).
- [44] P. W. Anderson, Phys. Rev. B **78**, 174505 (2008).
- [45] P. W. Anderson, P. A. Casey, Phys. Rev. B **80**, 094508 (2009).
- [46] P. A. Casey, P. W. Anderson, Phys. Rev. Lett. **106**, 097002 (2011).
- [47] P. Phillips, Ann. Phys. (N.Y.) **321**, 1634 (2006).
- [48] P. Phillips, Rev. Mod. Phys. **82**, 1719 (2010).
- [49] S. Chakraborty, D. Galanakis, P. Phillips, Phys. Rev. B **78**, 212504 (2008).
- [50] S. Chakraborty, P. Phillips, Phys. Rev. B **80**, 132505 (2009).
- [51] Y. Z. You, I. Kimchi, A. Vishwanath, (arXiv:1109.4155).
- [52] R. Shankar, A. Vishwanath, (arXiv:1106.0015).
- [53] P. Hosur, S. Ryu, A. Vishwanath, Phys. Rev. B **81**, 045120 (2010).
- [54] A. D. Arulsamy, Physica C **356**, 62 (2001).
- [55] A. D. Arulsamy, Phys. Lett. A **300**, 691 (2002).
- [56] A. D. Arulsamy, Transport Theory in the Normal state of high- T_c Superconductors, in *Superconductivity Research at the Leading Edge*, ISBN: 1-59033-861-8, Editor: P. S. Lewis (Nova Science Pub., N.Y., 2004, USA) pp. 45-57.
- [57] G. A. Dionicio, PhD thesis, The Technical University of Dresden, Germany (2006).
- [58] S. Fukuda, Y. Nakanuma, J. Sakurai, A. Mitsuda, Y. Isikawa, F. Ishikawa, T. Goto, T. Yamamoto, J. Phys. Soc. Jpn. **72**, 3189 (2003).
- [59] B. Leridon, A. Defossez, J. Dumont, J. Lesueur, J. P. Contour, Phys. Rev. Lett. **87**, 197007 (2001).
- [60] M. Sutherland, D. G. Hawthorn, R. W. Hill, F. Ronning, S. Wakimoto, H. Zhang, C. Proust, E. Boaknin, C. Lupien, L. Taillefer, R. Liang, D. A. Bonn, W. N. Hardy, R. Gagnon, N. E. Hussey, T. Kimura, M. Nohara, H. Takagi, Phys. Rev. B **67**, 174520 (2003).

- [61] A. D. Arulsamy, A. Soon, C. Stampfl, Transport properties of $\text{YBa}_2\text{Cu}_3\text{O}_7$ superconductors and electronic structure of Cu_2O surfaces, in *YBCO Superconductor Research Progress*, ISBN: 978-1-60456-083-1, Editor: L. C. Liang (Nova Science Pub., N.Y., 2008, USA) pp. 11-51.
- [62] A. D. Arulsamy, Ann. Phys. (N.Y.) **326**, 541 (2011).
- [63] A. Carrington, D. J. C. Walker, A. P. Mackenzie, J. R. Cooper, Phys. Rev. B **48**, 13051 (1993).
- [64] K. Q. Ruan, Q. Cao, S. Y. Li, G. G. Qian, C. Y. Wang, X. H. Chen, L. Z. Cao, Physica C **351**, 402 (2001).
- [65] S. J. Hagen, T. W. Jing, Z. Z. Wang, J. Horvath, N. P. Ong, Phys. Rev. B **37**, 7928 (1988).
- [66] H. Takagi, B. Batlogg, H. L. Kao, J. Kwo, R. J. Cava, J. J. Krajewski, W. F. Peck, Phys. Rev. Lett. **69**, 2975 (1992).
- [67] R. A. Cooper, Y. Wang, B. Vignolle, O. J. Lipscombe, S. M. Hayden, Y. Tanabe, T. Adachi, Y. Koike, M. Nohara, H. Takagi, C. Proust, N. E. Hussey, Science **323**, 603 (2009).
- [68] N. E. Hussey, J. Phys. Condens. Matter **20**, 123201 (2008).
- [69] A. D. Arulsamy, Phys. Lett. A **334**, 413 (2005).
- [70] A. D. Arulsamy, X. Y. Cui, C. Stampfl, K. Ratnavelu, Phys. Status Solidi B **246**, 1060 (2009).
- [71] A. D. Arulsamy, Submitted for publication, (arXiv:1105.5862) (2011).
- [72] A. D. Arulsamy, U. Cvelbar, M. Mozetič, K. Ostrikov, Nanoscale **2**, 728 (2010).
- [73] C. T. Chen, F. Sette, Y. Ma, M. S. Hybertsen, E. B. Stechel, W. M. C. Foulkes, M. Schuster, S. W. Cheong, A. S. Cooper, L. W. Rupp, Jr., B. Batlogg, Y. L. Soo, Z. H. Ming, A. Krol, Y. H. Kao, Phys. Rev. Lett. **66**, 104 (1991).
- [74] R. Mahendiran, S. K. Tiwary, A. K. Raychaudhuri, T. V. Ramakrishnan, R. Mahesh, N. Rangavittal, C. N. R. Rao, Phys. Rev. B **53**, 3348 (1996).
- [75] A. D. Arulsamy, K. Eleršič, M. Modic, U. Cvelbar, M. Mozetič, ChemPhysChem **11**, 3704 (2010).
- [76] P. Mahadevan, A. Zunger, Phys. Rev. B **68**, 75202 (2003).
- [77] M. J. Winter, (www.webelements.com). The Elements Periodic Table: Essential Data and Description.

E-mail address: sadwerdna@gmail.com

CONDENSED MATTER GROUP, DIVISION OF INTERDISCIPLINARY SCIENCE, 79-F-02-08 KETUMBAR HILL, JALAN KETUMBAR, 56100 KUALA-LUMPUR, MALAYSIA